*Q. J. R. Meteorol. Soc.* (1999), **125**, pp. 29–54

# The horizontal and vertical structure of east Asian winter monsoon pressure surges

By GILBERT P. COMPO[1]*, GEORGE N. KILADIS[2] and PETER J. WEBSTER[1]
[1]*University of Colorado at Boulder, USA*
[2]*NOAA Aeronomy Laboratory, Boulder, USA*

(Received 27 January 1997, revised 11 May 1998)

SUMMARY

East Asian cold-air outbreaks, accompanied by increasing surface pressure ('pressure surges'), are shown to be an important aspect of the subseasonal variability of the winter monsoon system. In this study the statistical linear relationship between pressure surges, tropical convection, and tropospheric circulation is assessed using a ten-year data set (1985/86–1994/95) of the European Centre for Medium-Range Weather Forecasts gridded operational analyses. From spectral analysis the pressure, wind, and temperature fluctuations indicative of strong pressure surges are found to have statistically-significant spectral peaks at submonthly periods (6 to 30 days). Linear regression analysis is used to detail the time evolution of the dominant horizontal and vertical structure of east Asian pressure surges. Surges are shown to relate significantly to circulation anomalies in both the meridional and zonal components of the lower-tropospheric wind. Relationships between east Asian pressure surges in the submonthly band and tropical circulation anomalies are found over the Bay of Bengal, the eastern Indian Ocean, Indonesia, and the western Pacific regions. Submonthly surges over the South China Sea are related to strong surges and convective activity south of Indonesia, over the South China Sea, the eastern Indian Ocean, and the Philippine regions. Surge-enhanced convective activity is found to precede an enhancement of the local east Asian Hadley cell. Submonthly surges over the Philippine Sea are related to periods of westerly-wind anomalies and convective activity in the western Pacific. Upper-level wave activity over western Asia precedes submonthly surges. The wave activity amplifies in the region of the Pacific jet stream, and can be traced dispersing equatorward through the region of upper-level westerlies over the eastern tropical Pacific.

KEYWORDS: Cold surges Pressure surges Shelf waves Tropical–extratropical interaction

## 1. INTRODUCTION

During the east Asian winter monsoon, periods of strong northerly winds and anomalously low temperatures dominate the synoptic weather from Siberia to the South China Sea. Although different definitions of these so-called 'pressure surges' have been proposed, (e.g. Boyle and Chen 1987), consensus exists on a few important characteristics in the region of east Asia; a sharp drop in temperature is accompanied by a strengthening of the climatological northerly winds and an increase in surface pressure. As enumerated by Boyle and Chen, surges have been defined by arbitrary thresholds of 12- to 24-hour temperature changes, wind acceleration, wind speed, surface pressure changes, and station-pressure differences. Absolute agreement on a definition for surges is difficult to find, probably because east Asia is an extensive area and individual researchers construct definitions based on the local response to the surge. East Asian pressure surges are also termed 'cold surges' because a decrease in temperature as far south as 17°N accompanies the increasing pressure and northerly winds (Chang *et al.* 1983). Wu and Chan (1995) preferred the term 'northerly surge' to highlight the increase in wind speed that is predominantly from the north. In studying the tropical–midlatitude relationship during surge events the term 'pressure surge' is probably more applicable as it will be shown that, while these events do not always bring significant near-surface temperature perturbations to the near-equatorial tropics, they are usually associated with non-negligible changes in the tropical pressure and wind fields.

* Corresponding author: Cooperative Institute for Research in the Environmental Sciences, University of Colorado, Boulder, CO 80309–0449, USA. e-mail: gpc@cdc.noaa.gov

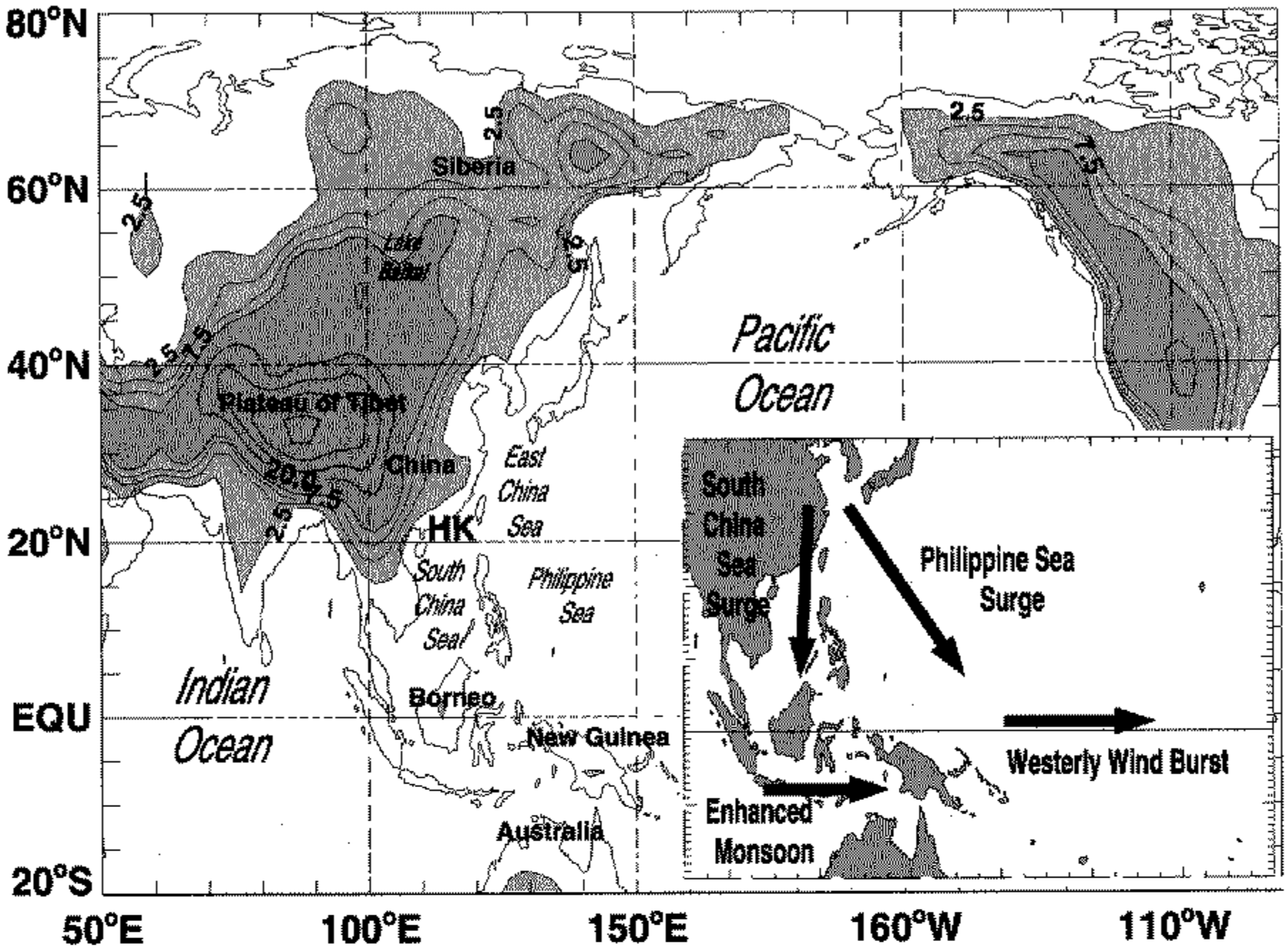


Figure 1. Map of smoothed orography at 2.5° resolution. The contour interval is 2.5 hm until 10 hm (light grey shading), and 100 hm thereafter (dark grey shading). Geographical features referenced in the text are indicated. The inset shows the regions that previous studies have indicated for surge activity and related tropical variability.

Two separate east Asian regions, the Philippine Sea and the South China Sea, frequently experience occurrences of strong pressure surges (Fig. 1). Both regions represent separate, preferred, paths for surges. Between these two principal loci is a relative minimum in surge occurrence, with separate local maxima of days with strong northerly winds occurring over the South China Sea and Philippine Sea during the boreal winter (Ding 1990). The separate local maxima of days of strong northerly winds has been reproduced in an atmospheric general-circulation model (AGCM) study of pressure surges (Slingo 1998). As pressure surges approach the equator, some are followed by an increase in tropical convective activity in both regions (Williams 1981; Chu 1988; Weickmann and Khalsa 1990; Kiladis *et al.* 1994; Meehl *et al.* 1996).

The life cycles of surges over the South China Sea have received considerably more attention than those over the Philippine Sea. A summary of the conclusions involving South China Sea surges is given below:

(i) *Surges originate in the midlatitudes* . A baroclinic disturbance in the region of Lake Baikal (Fig. 1) develops prior to a surge occurrence. The associated upper-level wave subsequently strengthens in the Pacific jet region (Chang and Lau 1982; Joung and Hitchman 1982; Lau and Lau 1984; Hsu 1987). Baroclinicity is enhanced prior to surge activity by an unusually strong Siberian high (Ding 1990; Wu and Chan 1995, 1997). The east Asian jet stream accelerates and extends eastward prior to, and during, the surge arrival at Hong Kong (Chang and Lau 1980, 1982; Lau *et al.* 1983; Chang and Lum 1985) . The initial acceleration results from midlatitude baroclinic processes while the subsequent strengthening may be a feedback from surge enhancement of tropical convection (Chang and Lum 1985). However, during surges the jet may strengthen on its own due to baroclinic and

barotropic processes without any forcing from the tropics (Chang and Chen 1992). Hsu *et al.* (1990) and Meehl *et al.* (1996) have suggested that some surges are a response to enhanced subtropical upper-level wave activity forced in part by convection in the eastern Indian Ocean.

(ii) *The surge arrival at Hong Kong is marked by dramatic 12- to 24-hour changes in synoptic conditions* . Surges at Hong Kong bring decreased near-surface temperatures and dew points, increased surface pressures, and strong northerly winds within a period of 12–24 hours. The exact timing of changes depends on the definition used (Chang *et al.* 1983; Wu and Chan 1995).

(iii) *Surge passage is a two-stage process* . A fast southward moving (about 40 m $s^{-1}$) pressure pulse is followed by a slower moving (10 to 15 m $s^{-1}$) pressure increase (Chang *et al.* 1983; Leathers 1986). The second pressure rise is accompanied by a frontal passage with drops in near-surface temperature and humidity and strengthening of the climatological northerly winds. Over the Asian land mass the pressure pulse has characteristics similar to an orographic Kelvin wave, whose restoring forces are gravity and the Coriolis effect normal to a barrier (Leathers 1986; Tilley 1990; Reason 1994). Over the South China Sea, the fast moving pulse has been identified as a gravity wave (Chang *et al.* 1983; Webster 1987). The second pressure increase and associated frontal passage have been modelled as a topographic Rossby wave, the atmospheric analogue to the oceanic shelf wave (see Mysak (1980) for a review of the oceanic case), whose restoring force is the orographically augmented gradient of potential vorticity along a sloping bottom surface (Leathers 1986; Hsu 1987; Tilley 1990). In contrast, Colle and Mass (1995) have suggested that Rocky Mountain surges, which appear to be similar to South China Sea surges, are governed by nonlinear advection, rather than by orographic Kelvin-wave or shelf-wave dynamics.

(iv) *The east Asian meridional divergent circulation is enhanced* . The east Asian meridional divergent circulation, the so-called 'local Hadley cell', is enhanced in a thermally-direct sense during the entire surge event, with maximum amplitude following the surge passage over southern China (Chang and Lau 1980, 1982; Chu and Park 1984; Davidson *et al.* 1984; Chang and Lum 1985; Chang and Chen 1992). Concurrently, upper-level divergence over the South China Sea increases. Researchers disagree on the latitudinal extent of the enhancement, however. Chang and Lau (1982) presented evidence that the local Hadley cell was noticeably enhanced prior to a surge, while Wu and Chan (1997) recently suggested that the enhancement of the local Hadley cell follows a surge. Wu and Chan, however, did not analyse the divergent wind directly and may, therefore, have been examining a primarily rotational response to a surge.

(v) *Surges coincide with an increase in convective activity in the South China Sea region* . Separate studies show that following surge passage over southern China, convective activity frequently increases in amplitude and areal extent over several areas: north of Borneo, along the Indo-China coast, over the central South China Sea, and over the Philippine archipelago (Ramage 1971; Chang *et al.* 1979; Chang and Lau 1980, 1982; Murakami 1980; Houze *et al.* 1981; Johnson and Priegnitz 1981; Lau 1982; Kiladis *et al.* 1994; Meehl *et al.* 1996).

(vi) *The Australian monsoon becomes active following a surge passage through southern China* . Australian monsoon westerlies and convection often increase 2–3 days after a surge passage is detected at stations along the southern Chinese coast (Murakami 1980; Webster 1981; Williams 1981; Love 1985a; Webster 1987). However, McBride (1987) found no obvious association between tropical cyclones, an important component of monsoon

activity, and surge occurrence for the Winter MONEX* year. In contrast, Love (1985b) presented a composite study and case analysis of east Asian surges that suggests surges do appear to have an effect on southern hemisphere tropical cyclogenesis north of Australia.

Many of the conclusions reached about South China Sea surges depend on different data sets which extend over different time periods. In many of the composite studies performed, the use of different surge definitions leads to completely different surge statistics even within the same year (Boyle and Chen 1987). Several of the studies depend on data from the Winter MONEX, which was a weak year for surge activity (Lau and Chang 1987) and, thus, may not accurately represent the surge relationship to tropical activity in general. A study that is independent of definition is needed to find the basic relationships between variables associated with east Asian pressure surges.

The sequence of events associated with surge passage over the South China Sea or Philippine Sea occurs on a wide range of temporal scales with periods from 4 days to 30 days (Murakami 1979; Ding 1990; Kiladis *et al.* 1994; Meehl *et al.* 1996). Using data for the period 16 November 1970 to 15 March 1971, Murakami (1979) found spectral peaks are prominent in the meridional wind and in the latitudinal pressure gradient at synoptic (two- to six-day) time-scales over the East China Sea, the main path for Philippine Sea pressure surges. Murakami also found large power on this time-scale in the meridional wind over the South China Sea. In addition, meridional-wind and surface pressure time series over the South China Sea have a spectral peak between 20 and 30 days. In the present study, the spectral analysis of surges is extended by using ten winters (December–April), allowing greater confidence in the results. The statistical significance of the spectra is also discussed.

Another important time-scale in the tropics is that of the Madden–Julian oscillation (MJO), or 40- to 50-day oscillation (see Madden and Julian (1994) for a review of the phenomenon). Some researchers have shown a connection between strong pressure surges and the movement of convection between the eastern Indian Ocean and the western Pacific Ocean associated with the MJO. (e.g. Weickmann and Khalsa 1990). Hsu *et al.* (1990) documented a case of a pressure surge occurring in response to a subtropical wave-train in the western Pacific forced by MJO convection in the eastern Indian Ocean. The Indonesian convection activated by the pressure surge was thought to be enhanced by favourable upper-level conditions that developed as part of the MJO.

To provide an example of the variability of pressure fluctuations over east Asia, a time–latitude diagram along 110°E of sea-level-pressure (SLP) departures from the climatological seasonal cycle is shown in Fig. 2. This longitude is representative of the region from 105°E to 115°E. Using the 5.0 hPa anomaly contour as a reference, Fig. 2 shows that positive pressure anomalies along east Asia have their origin well north of 50°N, and can be traced as far south as 10°N. Negative anomalies also appear to be propagating southwards. Phase lines (solid lines, Fig. 2) are drawn on the diagram, and several examples are labelled. There appear to be two classes of anomalies based on southward propagation speeds of 22 m $s^{-1}$ for some shorter duration events, and on 13 m $s^{-1}$ for others of longer duration. These speeds appear to represent the movement of both negative and positive anomalies. The faster-speed anomaly (labelled C) appears to have a time-scale of less than six days and only a weak perturbation south of 20°N. A linear regression analysis of two- to six-day (synoptic) bandpass filtered anomalies (not shown) indicates that the faster-propagating pressure anomalies shown in Fig. 2 can be associated with synoptic-time-scale perturbations that appear to be well-described as midlatitude baroclinic disturbances. Surges on the synoptic time-scale have been examined in detail by Lau and Lau (1994). They found that

* MONsoon EXperiment, a component of the World Climate Research Programme

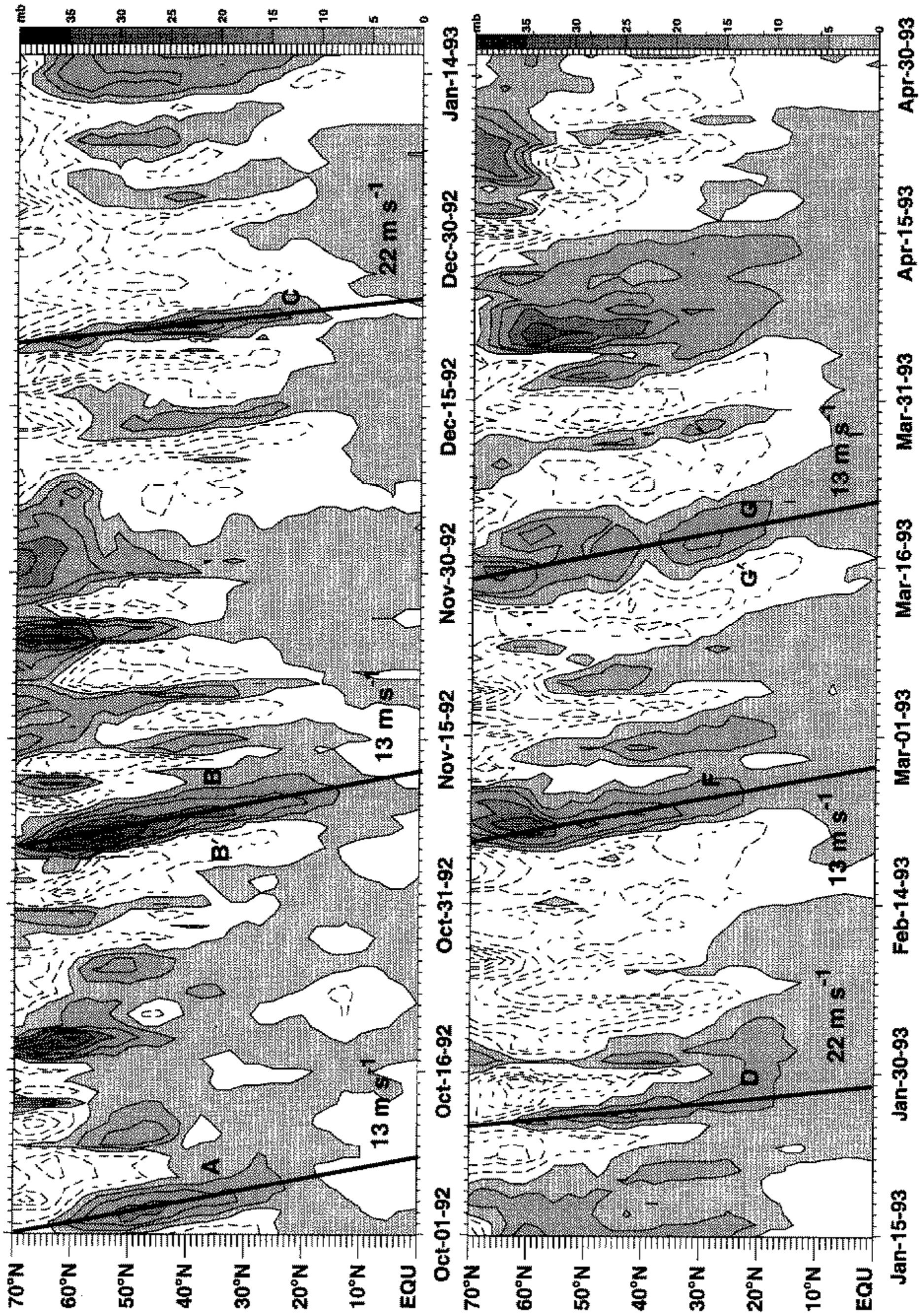


Figure 2. Hovmöller (latitude versus time) diagram along 110.0°E of sea-level pressure anomalies. Anomalies are computed by subtracting a three-harmonic climatological annual cycle from the original time series, as described in the text.

the dynamics and energetics of these synoptic-time-scale surges were largely like those of midlatitude baroclinic disturbances. In the present study, we turn our attention to the slower-propagating anomalies. As will be shown in section 4, the slower speed can be identified with submonthly (6 to 30 days) time-scale surges.

Philippine Sea pressure surges have received less attention, perhaps because they would seem to have less human impact than surges along the densely populated coast of the South China Sea. However, some investigators have shown a relationship between these more eastern pressure surges and the so-called 'westerly wind bursts' (Chu 1988; Chu and Frederick 1990; Kiladis *et al.* 1994; Meehl *et al.* 1996). These episodes of near-surface enhanced westerlies in the equatorial western Pacific represent a major perturbation to both the atmosphere and the ocean. Westerly wind bursts are sometimes associated with pairs of symmetric tropical cyclones forming on both sides of the equator (Keen 1982). Groups of westerly wind bursts may interact with interannual modes of variability such as the El-Niño Southern Oscillation (ENSO), with westerly bursts in the central Pacific increasing in frequency during the warm phase of ENSO (Murakami and Sumathipala 1989). Oceanic mixing in the western Pacific is increased during periods of the enhanced winds associated with westerly bursts (Lukas and Lindstrom 1991; McPhaden *et al.* 1988, 1992) . Oceanic equatorial Kelvin waves, which have been hypothesized to play a role in ENSO initiation, have been shown to be initiated by westerly bursts (Knox and Halpern 1982; Giese and Harrison 1990; Kindle and Phoebus 1995).

Despite the advances made in previous studies, a number of important questions remain:

- *What are the time-scales associated with surge activity?*
- *What are the basic relationships between surge-associated variables, independent of an arbitrary definition?*
- *Is the tropical response to pressure surges a robust signal?*

In the present study, by addressing the questions above, we hope to extend understanding of the spatial and temporal variability related to episodes of east Asian pressure surges. This paper is organized as follows. Section 2 discusses the data and provides a rationale for the analysis methods used. The time-scales present in pressure-surge variables are identified through spectral analysis in section 3. A linear regression analysis is presented in section 4. We discuss the horizontal and vertical structure of east Asian pressure surges, the relationship of surges to fluctuations in the east Asian jet streams and upper-level baroclinic wave activity, and the correlation between pressure surges and tropical variability in tropospheric circulation and convection. Discussion and comparison with previous work is presented in section 5.

## 2. Data and methodology

### (*a*) *Data*

The European Centre for Medium-Range Weather Forecasts (ECMWF) gridded global analyses of standard atmospheric variables are used for the period 1 January 1985 to 31 December 1995 to examine east Asian winter monsoon pressure surges. For a detailed description and analysis of this data set see Trenberth (1991, 1992) and Trenberth and Guillemott (1995). The twice-daily ECMWF analyses are averaged to remove diurnal fluctuations, prior to any other processing. A daily outgoing long-wave radiation (OLR) dataset produced by the National Oceanographic and Atmospheric Administration (NOAA) for the same time period is also used to represent tropical convective activity.

For a description of the interpolation scheme used on the OLR data set see Liebmann and Smith (1996). Both data sets are on an identical 2.5° by 2.5° latitude–longitude grid.

### (*b*) *Methodology*

Anomaly time series are constructed by removing the first three harmonics (periods of 365.25, 182.625, and 121.75 days) of the climatological seasonal cycle using a least-squares fit to the entire record of 1 January 1985–31 December 1995. To determine if any significant periodicities occur in the time series, ten-winter ensemble averages of spectra are computed using 181 days from 15 November to 15 May with a 15-day cosine taper on each end. All spectral estimates presented are the average of spectral values over three adjacent frequencies.

Confidence levels for the spectral calculations are determined with Monte Carlo tests assuming a first-order Markov process. At each grid point, and for each winter period, 1000 autocorrelated random time series are constructed, using the lag–1 autocorrelation of the anomaly data of that winter. The spectrum for each random time series is computed. The ten winters are averaged together to produced 1000 ensemble averages at each grid point. A distribution of spectral power is then calculated separately at each frequency and compared with that of the actual data. Statistical significance is then determined by comparing the actual spectral estimate with the 95% level of the distribution.

After examining spectral results, we find significant power at periods between 6 and 30 days in several of the variables associated with surge activity. The choice of this band also removes much of the high-frequency baroclinic wave activity in the midlatitudes, the high-frequency mixed Rossby–gravity wave activity in tropics, and the lower-frequency fluctuations associated with the MJO. The complete record of the anomaly data is temporally filtered into a submonthly (6–30 day) frequency band using a Lanczos digital filter (Duchon 1979) with 121 daily weights. The high number of weights helps eliminate Gibb's ringing in the response of the filter. The response of the filter used is shown in Kiladis and Weickmann (1992). These are the same bands and weights as used in several previous studies, so the results shown here are directly comparable to those works (Kiladis and Weickmann 1992; Kiladis *et al.* 1994; Meehl *et al.* 1996).

The composite relationship between pressure surges and global circulation is determined using the linear-regression technique of Kiladis and Weickmann (1992). This approach assesses the statistically-significant linear relationship between SLP fluctuations indicative of surges and the global circulation and convective variability. The bandpass-filtered SLP at various base points is cross-correlated and linearly regressed against identically filtered OLR and ECMWF-analysed SLP, wind, and temperature. A separate regression relationship is obtained for each variable at every grid point.

The analysis is first performed for base points covering east Asia. Regressions are separately computed using only three months of each year during the northern hemisphere cool season (September to November (SON), October to December (OND), November to January (NDJ), December to February (DJF), January to March (JFM), February to April (FMA), March to May (MAM)) for base points spaced every 10 degrees from 50°N to 10°S and from 100°E to 150°E (42 points), and are compared to determine the seasonality of pressure surges. The regressed patterns for SON and OND were decidedly different from the other three-monthly groupings. The northern-hemisphere tropical and midlatitude patterns seen for all of the three-monthly groupings DJF to FMA were quite similar. Given these results, the December to April data, inclusive, are used to obtain results shown here.

Regression of the filtered SLP predictor at a base point against the data at all other grid points permits the local statistical significance of the linear relationship between the SLP anomaly at the base point and the circulation or OLR anomaly to be determined using a

Student's $t$-test. The number of degrees of freedom at each grid point is derived according to the method of Livezey and Chen (1983). The time-lagged regression is also utilized to provide the temporal evolution of the large-scale-circulation and convective anomalies associated with the pressure perturbations. In this way, circulation anomalies that precede surges, and those that follow surges, can be determined objectively. Wind vectors are plotted where the local correlation of either the zonal $u$ or meridional $v$ wind component meets or exceeds the 99.5% confidence level, while the regressed OLR is mapped only at those locations that meet or exceed the 99.5% confidence level. Contours of SLP and stream function are shown without regard to correlation.

The use of the regression method assumes a nearly linear relationship between the predictor and predictand. A nearly linear relationship between the SLP, the circulation, and the wind during pressure surges is apparent in case studies of pressure surges (Chang *et al.* 1983; Chu and Park 1984; Love 1985a). With respect to OLR, the linear assumption is valid to the extent that lower-tropospheric wind anomalies associated with pressure surges contribute to convective activity. A direct relationship between pressure-surge occurrence, with its accompanying increase in the north-easterly flow over the South China Sea, and an increase in convective activity is observed in case studies (Houze *et al.* 1981; Johnson and Priegnitz 1981). However, nonlinear interactions, where the feedback of the circulation onto the convection itself might be important (e.g. Chang and Lim 1988), are a likely component of the response to the tropical heating anomaly induced by the pressure surges.

Two base points are shown as representative of the results obtained using a total of 42 separate SLP base points throughout the east Asian sector. The results highlighted here are qualitatively insensitive to the choice of base point. The South China Sea base point at (15°N, 115°E) represents the northernmost predictor in the region of the South China Sea and continental east Asia that retains a statistically-significant relationship to southern hemisphere anomalies south of Indonesia, whereas the northern-hemisphere tropical-circulation and convective anomalies are robust and statistically significant using base points as far north as 50°N over the Asian continent. The regression results at this base point are plotted using a +3.0 hPa anomaly, an anomaly value based on the magnitude of strong surges observed at this latitude (e.g. cases B, F, and G in Fig. 2). Similar magnitudes of SLP anomalies at this latitude are seen in the composite results of Wu and Chan (1995). The Philippine Sea base point (20°N, 140°E) provides a secondary verification of the reproducibility of the signals observed west of 120°E using the South China Sea base point. Further, a significant relationship observed between Philippine Sea base points and circulation and OLR anomalies in the equatorial western Pacific is not observed with any base points located over continental east Asia or the South China Sea. A Philippine Sea base point is therefore included to illustrate this association. The regression results at the Philippine Sea base point are plotted assuming an anomaly value of +4.0 hPa, which is also consistent with observed cases of surges in this area (not shown).

## 3. Spectral analysis

Figure 2 displays variations of SLP anomalies on several time-scales. To test the generality of the limited time period examined, the spectral characteristics of the ten-year sample are investigated. Figure 3 shows the latitudinal distribution of SLP spectral power during boreal winter along 110°E. This meridian covers the western South China Sea and coastal Indo-China. North of 35°N, significant power at the 95% level is seen for periods less than 9 days. In the subtropics and tropics, these synoptic-scale peaks diminish in intensity, while the amplitude of the peaks in the submonthly and MJO bands increase. The small regions of significant power seen for periods less than nine days south of 10°N

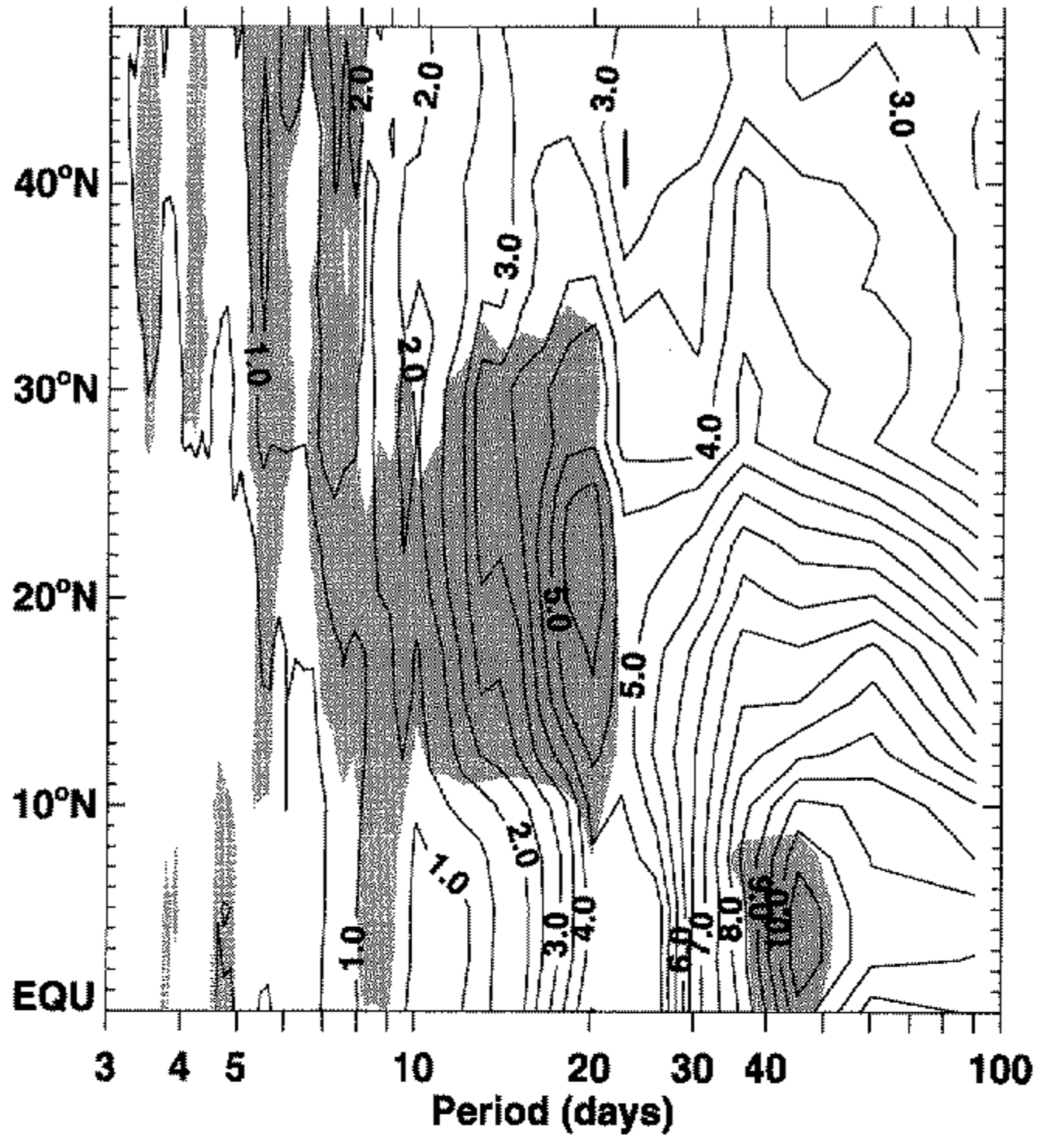


Figure 3. Ten-winter ensemble spectra of anomalous sea-level pressure along 110°E representative of South China Sea pressure surges. The time period employed is November 15 to April 15 of 1985/86 to 1994/95. The line contours represent the per-cent variance in the spectrum at each latitude. The shading represents the regions that exceed the 95% confidence levels from Monte Carlo tests. The units are per cent of total variance. The contour interval is 0.5%.

appear quite well separated from those in the midlatitudes, reflecting the lack of deeply penetrating surges at the synoptic time-scale seen in Fig. 2. A peak at around 20 days dominates the spectra from 40°N to the equator, with the 95% significant region largely between 35°N and 10°N. Although not statistically significant until near the equator, there is a broad peak in power between 30 and 70 days at most latitudes that is statistically significant between 40 and 50 days south of 7.5°N; this is most likely to be associated with the MJO.

As with SLP, spectra of lower tropospheric air temperature between 105°E and 120°E (not shown) exhibit a decrease in significant power at synoptic time-scales from the mid-latitudes to the deep tropics. Also, like the SLP, the air temperature at 850 hPa has a significant spectral peak around 20 days from 35°N to 15°N. Similarly, 850 hPa meridional-wind spectra along 110°E south of 15°N (not shown) have noticeable peaks between 10 and 20 days, though significant at only the 90% level. A coherent large-scale relationship between pressure, air-temperature, and circulation anomalies associated with pressure surges on the submonthly time-scale is demonstrated in the regression analysis of section 4.

To compare the spectral characteristics of SLP in the South China Sea surge area with that in the Philippine Sea, Fig. 4(a) shows spectra of SLP as a function of longitude along 20°N. This latitude represents the zonal band influenced by both Philippine Sea and South China Sea surges. Only periods between 3 and 25 days are shown; most of the SLP variance significant at the 95% level is in this range over the South China Sea (Fig. 3), and this is also true further east. The dominance of the submonthly spectral peaks at around 20 days is apparent from 95°E to 140°E. The two separate maxima in this band at 105°E

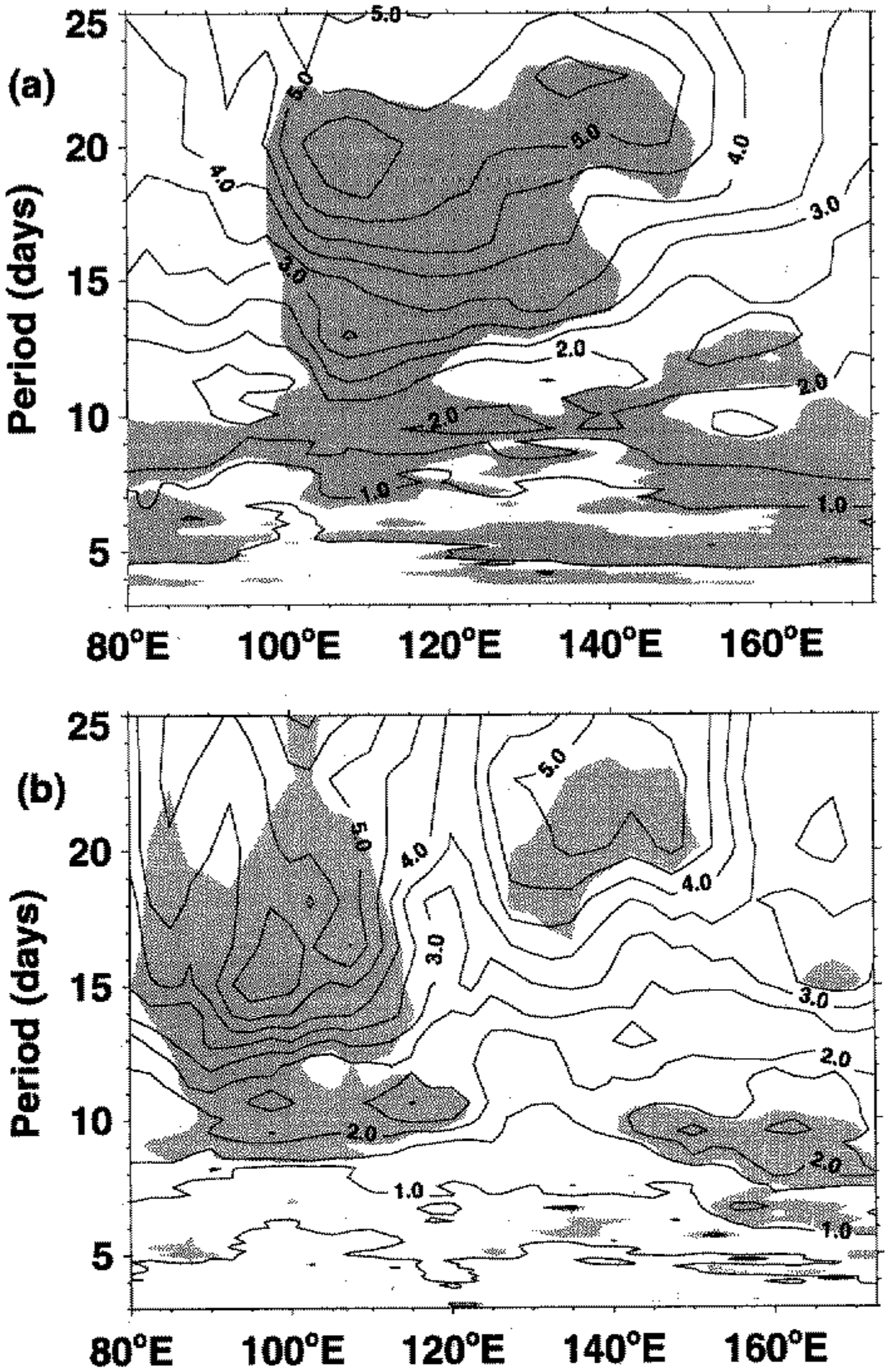


Figure 4. As Fig. 3 but for (a) anomalous sea-level pressure along 20°N and (b) 850 hPa zonal wind along 7.5°N.

and 135°E, with a spectral gap in between, probably demonstrate the two preferred paths for pressure surges.

Zonal-wind spectra at lower latitudes show the two separate maxima of submonthly power over these regions, as exemplified in Fig. 4(b) showing the spectra along 7.5°N as function of longitude. Figure 4(b) shows that zonal-wind fluctuations over the South China Sea have significant power at the 95% level at nearly the same periods of the submonthly band as the SLP fluctuations to the north (Fig. 4(a)). Submonthly peaks between 10 and 20 days are largely confined to the South China Sea and Bay of Bengal while the Philippine Sea has significant power at 22 days centred at 140°E. The concomitant significant spectral peaks between SLP and zonal wind imply that, in the deep tropics, pressure surges affect the zonal wind, in addition to the meridional-wind signal that has been emphasized in some studies (e.g. Ramage 1971; Lau 1982; Chang *et al.* 1983; Lau *et al.* 1983; Wu and Chan 1995; Zhang *et al.* 1997) . The relative lack of power at greater than 30 days and less than 6 days, along with the results of Fig. 2, indicates that 6- to 30-day filtering is

appropriate for capturing the majority of the significant variance associated with the wind, temperature, and SLP over east Asia.

## 4. Linear-regression analysis

Based on the results of the previous section, pressure-surge variability in the 6- to 30-day band is examined.

### (*a*) *Lower-tropospheric circulation*

In Fig. 5, the lower-tropospheric circulation anomalies associated with the evolution of submonthly pressure surges are examined using an SLP base point at 15°N, 115°E. Five days prior to the peak in pressure at the base point (Fig. 5(a)) positive pressure anomalies cover northern Asia with a wedge of positive pressure and northerly-wind anomalies extending over most of China. The leading edge of the anomaly is marked by the thick dark line (0.5 hPa). Suppressed convective activity is shown over, and east of, the Philippines and south of India.

At day –2 (Fig. 5(b)), the surge has crossed the equator and low-level convergence just south of Borneo is indicated by a statistically-significant increase in convective activity, as shown by negative values of OLR (shading). Divergence calculations (not shown) on the 850 hPa regressed field also confirm convergence collocated with the negative OLR anomaly. In addition, convective activity is also enhanced over Indo-China. Note the large amplitude easterly component in the regressed north-easterly wind anomalies over the southern portion of the South China Sea. The large amplitude confirms the relationship suggested in Fig. 3, that surge anomalies in the deep tropics have significant zonal, as well as meridional, wind perturbations. Convective activity increases in intensity in the region south of Borneo from day –5 to day –2 as low-level westerly anomalies appear to follow the convection, strengthening further from day –2 to day 0 (Fig. 5(c) and (d)). Anomalous convective activity over the southern Philippines and Philippine Sea is accompanied by statistically-significant low-level easterlies. North-east of Borneo and over south-east Asia, convective anomalies have also developed in the increasing north-easterly anomalies. By day 0, significant easterly anomalies also cover the Bay of Bengal and central India.

By day +3 (Fig. 5(d)), the South China Sea surge has weakened, while a positive pressure anomaly has propagated eastward from the China coast, extending the maximum of the enhanced tropical trades eastward and northward. The southerlies seen over China at day +3 expand southward by day +5 (Fig. 5(e)), at which time the surge anticyclone has weakend but convective activity is still indicated south of India.

It is observed that OLR anomalies over and around the South China Sea basin are significantly correlated to SLP using any base point along the path of pressure surges from 55°N to the equator in the longitude range of 105°E to 155°E (not shown). In contrast, OLR anomalies south of the equator in the eastern Indian Ocean and south of Borneo only correlate significantly with base points in the South China Sea, Philippine Sea, and East China Sea and do not correlate significantly with SLP fluctuations north of 20°N and west of 120°E, the land areas of mainland China and western Central Siberia. Tropical and deep tropical SLP base points show results similar to that of Fig. 5. These results indicate that many surges do not penetrate far enough south to affect southern-hemisphere westerlies and convection.

A significant relationship between SLP anomalies in the Philippine Sea and convective and wind anomalies in the equatorial western Pacific is observed in Fig. 6 using a base point located in the Philippine Sea (20°N, 140°E). Qualitatively similar results to those of Fig. 6 were obtained using base points throughout the Philippine Sea domain and into the

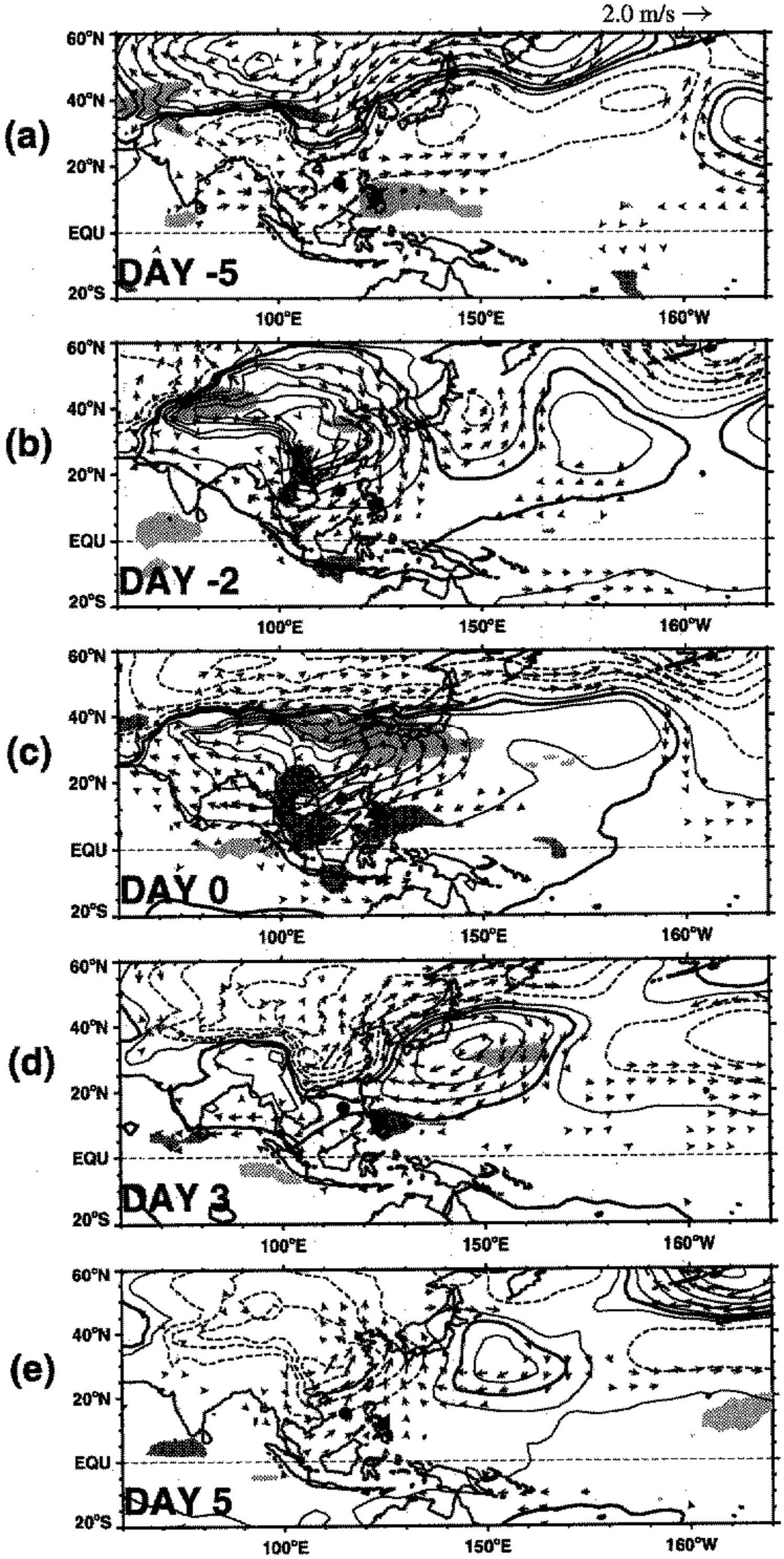


Figure 5. 6- to 30-day bandpass filtered sea-level pressure (SLP), outgoing long-wave radiation (OLR), and 850 hPa wind-anomaly fields linearly regressed against SLP at 15°N, 115°E (indicated by the black dot) for (a) 5 days preceding the maximum SLP anomaly at the base point, (b) 2 days preceding, (c) day of maximum, (d) 3 days after and (e) 5 days after. The vectors and the OLR are indicated at the local 99.5% significance level. Regressed values are based on a typical perturbation of SLP at the base point (3.0 hPa). SLP is plotted at a contour interval of 1.0 hPa (0.5 hPa included, positive thickened). The OLR contour is 8.0 W $m^{-2}$ with negative (positive) anomalies shaded dark (light) grey. Only every other wind-anomaly vector is plotted.

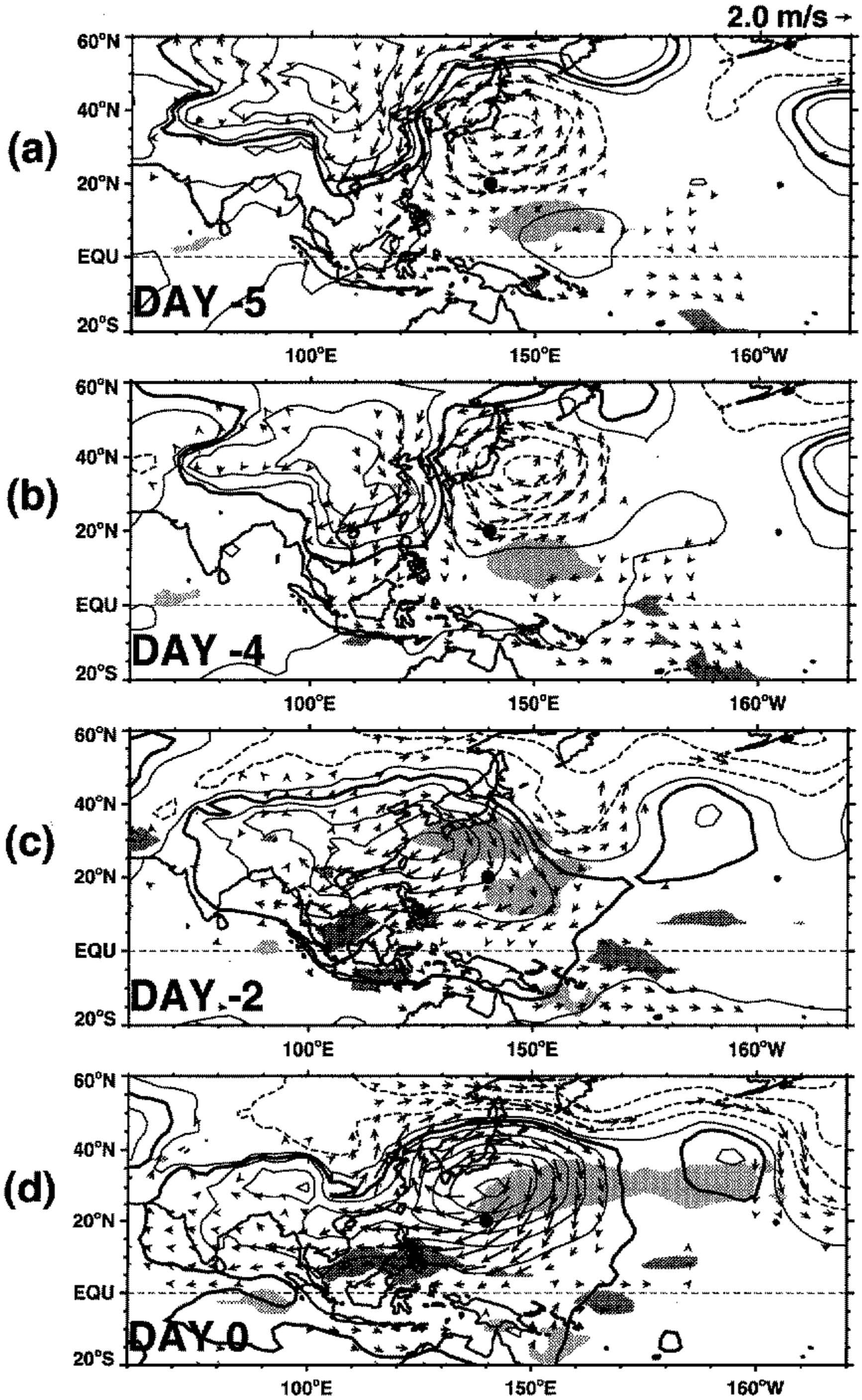


Figure 6. As Fig. 5 but for a sea-level-pressure (SLP) base point at 20°N, 140°E (indicated by the black dot). (a) 5 days preceding the maximum SLP anomaly at the base point, (b) 4 days preceding, (c) 2 days preceding and (d) day of the maximum. The regressed values are based on a 4.0 hPa anomaly at the base point.

East China Sea as far north as 40°N. The evolution of the anomalies in Fig. 6 west of 120°E is quite similar to that of Fig. 5 with a two- to three-day lag between the strongest pressure perturbations at the Philippine Sea base point compared with the South China Sea base point. However, the presence of significant anomalies in the tropical western and central Pacific in Fig. 6 is rather different and merits further consideration. The circulation and OLR anomalies in the equatorial central and western Pacific observed in Fig. 6 appear to precede the South China Sea surge and Philippine Sea surge. A positive OLR anomaly in the Philippine Sea at day –5 (Fig. 6(a)) propagates north-westward through the sequence and is still evident as a zonally oriented band along 30°N on day 0. In Fig. 6(d) the development of a large-scale pressure anomaly over the Philippine Sea and South China Sea produces a north-easterly trade surge from 160°E extending into the Bay of Bengal while equatorial westerly wind anomalies are present to the south of Indonesia and in the western Pacific.

The westerly-wind and OLR anomalies south of Indonesia observed in Fig. 6 appear to develop in a similar way to those observed in Fig. 5. However, the equatorial western Pacific wind anomalies seen at day –2 (Fig. 6(c)) appear to have had a tropical precursor. In the central equatorial Pacific, westerly anomalies are present at day –5 (Fig. 6(a)), well in advance of the south-eastward propagating extratropical pressure anomaly. These westerly-wind anomalies and associated negative OLR anomalies appear to propagate westward in Fig. 6, reaching maximum amplitude in the western Pacific at day –2 coincident with trade surge (Fig. 6(c)).

Figure 6 shows that the western Pacific near-equatorial anomalies appear to be propagating from the central Pacific to the western Pacific before a positive pressure anomaly is evident over the Philippine Sea. The evolution and structure of the central and western Pacific circulation and OLR anomalies in Fig. 6 are similar to those found by Kiladis and Wheeler (1995), who associated the structure with an equatorial Rossby wave.

The association between Philippine Sea surges and equatorial wind and OLR anomalies appears to arise from the combination of a westward moving tropical disturbance and a south-eastward moving midlatitude anticyclonic disturbance. By tracking the centres of the pressure anomalies from Fig. 6, the south-eastward propagation speed of the Philippine Sea anticyclone is approximately 7–8 m $s^{-1}$ while the tropical positive OLR anomaly and weak associated anticyclonic anomaly moves north-westward at approximately 3–4 m $s^{-1}$. The western Pacific westerly-wind anomalies appear to be enhanced by the pressure gradient arising from the Philippine Sea surge, but here are observed as coincident with the surge rather than a result of the surge. In contrast, the increase in the north-easterly trades is more directly attributable to the extratropical perturbations over the South China and Philippine Seas.

### (*b*) *Upper-tropospheric circulation*

Figure 7 shows the 200 hPa stream function and wind vectors obtained using the same SLP predictor as used in Fig. 5. The upper-tropospheric pattern related to pressure surges covers a broader area than that of the lower troposphere. On day –5 (Fig. 7(a)) most of the significant large-scale features are located over Asia. When compared with stream-function fields at lower levels (not shown) a westward tilt with height of the features is evident, indicative of baroclinic waves.

As convective anomalies develop over south-east Asia, the southern Philippines, and southern Sumatra from day –2 to day 0, a subtropical wave pattern is evident, arcing into the midlatitude jet-stream region of the central Pacific. By day +3 (Fig. 7(d)), as the convective signal weakens, the wave pattern advances further into the Pacific and the circulation centres over India diminish. The wave pattern propagating from Bangladesh

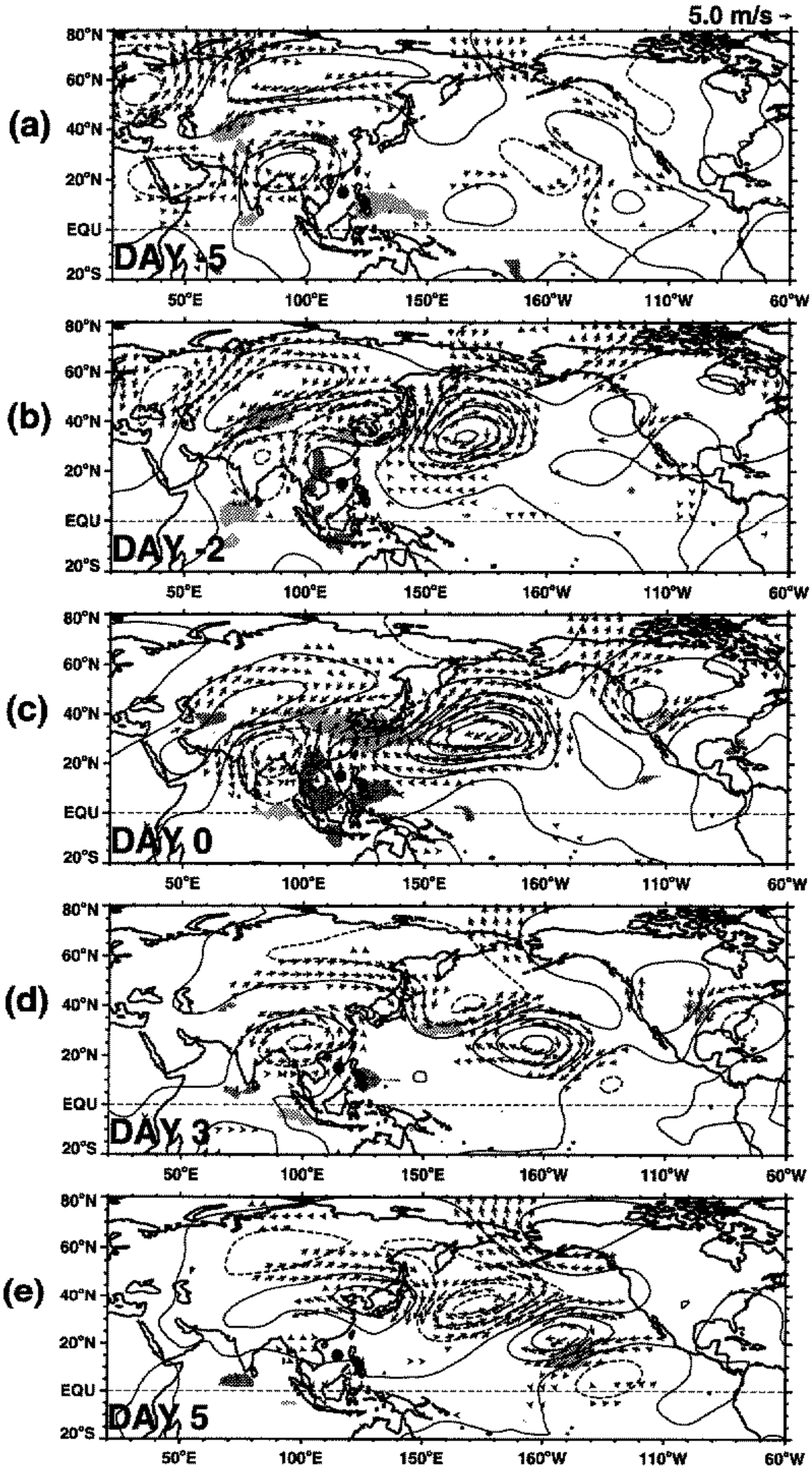


Figure 7. 6- to 30-day bandpass filtered outgoing long-wave radiation (OLR) and 200 hPa wind-anomaly fields corresponding to Fig. 5 for (a) 5 days preceding the maximum sea-level-pressure anomaly at the base point, (b) 2 days preceding, (c) day of maximum, (d) 3 days after, and (e) 5 days after. The minimum correlation coefficient for plotting the wind-anomaly vectors and the OLR is the 99.5% local significance level. The stream function is plotted without regard to the correlation with a contour interval of $3 \times 10^6$ m$^2$ s$^{-2}$. Only every other vector is plotted.

to the eastern tropical Pacific is similar to the results of observational studies that have examined the propagation of Rossby waves through westerly ducts in the eastern Pacific (Kiladis and Weickmann 1992; Tomas and Webster 1994). A similar wave pattern following a South China Sea surge has been simulated in an AGCM (Slingo 1998).

At day +5 (Fig. 7(e)) the wave pattern has significant anomalies crossing into the southern hemisphere, and suppressed convection is noted ahead of an upper-level trough at 150°W. In subsequent days (not shown) the trough observed in the central Pacific in Fig. 7(e) propagates equatorward and significant negative OLR anomalies develop in its poleward flow.

The upper-level north-westerly flow in the vicinity of Lake Baikal associated with an upper-level ridge is a key synoptic development in the initiation of pressure surges, and has been noted in previous studies (Chu 1978; Kung and Chan 1981; Boyle 1986; Boyle and Chen 1987). The results presented here indicate that upper-level north-easterly anomalies in the vicinity of Lake Baikal associated with a developing ridge over northern Siberia are present several days before a surge reaches the southern Chinese coast, while the north-westerly feature previously reported is not observed as a significant anomaly until one day before the surge reaches its maximum intensity. It should also be noted that the climatological upper-level flow in the vicinity of Lake Baikal is north-westerly (Boyle and Chen 1987; Zhang *et al.* 1997), and the previous studies have reported on observations of the total field.

While the lower- and upper-tropospheric flows are nearly vertically coincident over northern China on days prior to day –5 (not shown), at day –5 the lower-tropospheric north-easterly anomalies have advanced to southern China (Fig. 5(a)), while the upper-tropospheric anomalies remain poleward of 40°N (Fig. 7(a)). At day –2, the strong, statistically-significant north-easterly anomalies over the South China Sea seen in Fig. 5(b) have no corresponding 200 hPa circulation anomalies in Fig. 7(b). A statistically-significant 200 hPa anomaly over the South China Sea is not evident until day 0 (Fig. 7(c)).

In Fig. 7 the southerly flow is seen emanating from the convective region over western Indonesia toward the positive midlatitude OLR anomaly and the implied region of subsidence along 30°N. This suggests an enhanced local Hadley circulation during a surge. To further examine the evolution of the mass circulation, Fig. 8 compares regressed values of the 1000 hPa and 200 hPa divergence anomalies with the OLR anomaly at one of the grid points of strongest convective activity (5°N, 107.5°E). Figure 8 shows that the variations in the local east Asian Hadley cell are strongly correlated to the surface surge-induced variations in the divergent flow, with the surface changes leading the increase in the 200 hPa divergence of the local Hadley circulation by one day. Examination of the evolution of mapped values of OLR and divergence suggests that the timing is not an artifact of the propagation of the anomalies, nor of the near-equatorial grid point chosen (not shown). Upper-level southerlies follow the development of the OLR anomaly (Figs. 7(b) and (c)). Maps of the divergent part of the wind field indicate that these southerly anomalies have a strong divergent component (not shown). A region of positive OLR anomalies along northern China at 35°N marks the descending branch of the local Hadley cell (Fig. 7(c)). Together, Figs. 7 and 8 indicate that the Hadley cell is near mean strength preceding the surge, and that the upper-level local Hadley cell intensifies following a pressure surge. A consistent time delay between low-level convergence, convective activity, and upper-level divergence is seen with all base points employed (not shown).

### (*c*) *Propagation characteristics*

To quantify the southward propagation and magnitude of the South China Sea surge-associated perturbations, regressions of SLP and 850 hPa air temperature and meridional

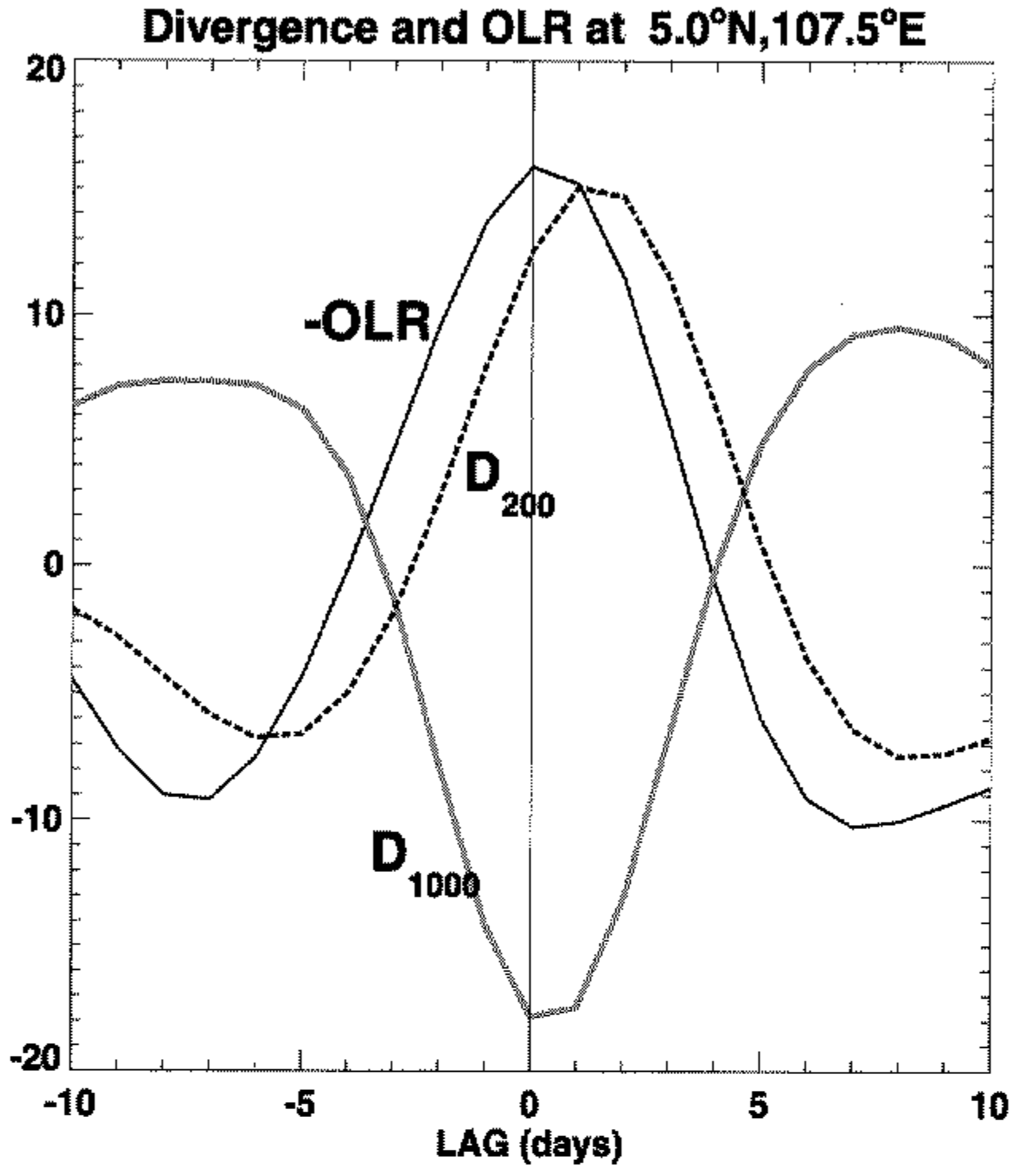


Figure 8. Time series versus lag of regressed values of 6- to 30-day bandpass filtered outgoing long-wave radiation (OLR) (black line), 1000 hPa divergence (grey line), and 200 hPa divergence (dashed line) anomalies at 5°N, 107.5°E regressed against sea-level pressure (SLP) at 15°N, 115°E (see Fig. 5). The regressed values are based on a realistic perturbation of SLP at the base point (3.0 hPa). The OLR is in units of W $m^{-2}$. The divergence is in units of $5.0 \times 10^{-6}$ $m^2$ $s^{-2}$.

wind are calculated as a function of lag and latitude, along 110°E using the South China Sea base point (15°N, 115°E) time series of SLP (Fig. 9). A positive pressure anomaly propagates southward at 8.9 degrees per day or 11.3 m $s^{-1}$, as indicated by the reference phase line, from the midlatitudes to approximately 15°N. The propagation speed changes south of 15°N to nearly 40 m $s^{-1}$ as the positive pressure increase crosses from 15°N to 5°S in one day. The two propagation speeds over east Asia are independent of the base point used.

The propagation of the temperature anomaly in Fig. 9(a) follows the pressure anomaly from 55°N to 10°N along 110°E. North of 55°N, the temperature anomaly is in quadrature with the pressure anomaly, consistent with eastward propagating baroclinic disturbances. South of 55°N however, the temperature and pressure anomalies are nearly in phase until they reach 15°N, where the rapid southward progression of pressure occurs. The 850 hPa air-temperature anomaly of 0.5°C penetrates to 7.5°N. The erosion of the near-surface negative-temperature-anomaly signal as the air passes over the South China Sea is discussed in the next section.

Chang *et al.* (1983) and Leathers (1986) discussed in detail two events associated with surges. The first event, a fast moving (40 m $s^{-1}$) positive pressure pulse was associated with a gravity-wave motion. The rapid southward propagation has been previously identified in other studies (Ramage 1971; Williams 1981; Webster 1987). Using a linear shallow-water model on a beta-plane, Lim and Chang (1981) and Zhang and Webster (1992) viewed surge effects over the South China Sea as the transient response of an adjustment to a

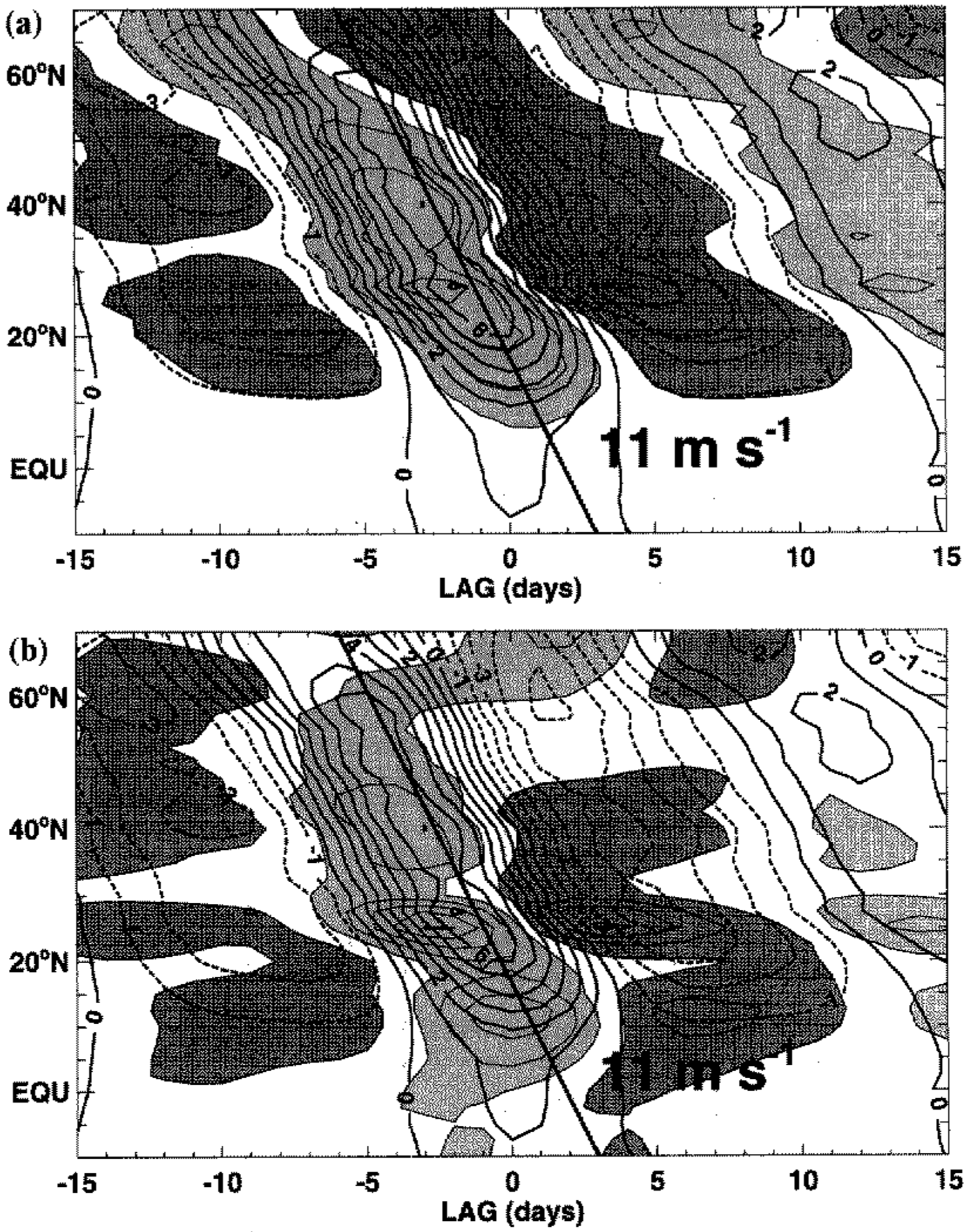


Figure 9. Latitude-versus-lag Hovmöller diagram along 110.0°E of regressed values of 6- to 30-day bandpass filtered sea-level pressure (SLP) anomaly (full lines, positive; dashed lines, negative) and (a) 850 hPa air temperature (the filled contour (dark grey, positive; light grey, negative) is 1.0°C starting at 0.5°C) and (b) 850 hPa meridional-wind (the filled contour (dark grey, positive; light grey, negative) is 1.0 m $s^{-1}$ starting at 0.5 m $s^{-1}$). The regressed values are based on a typical perturbation of SLP (3.0 hPa) at the base point (15°N, 115°E).

pressure–wind imbalance. Chang *et al.* (1983) attributed the rapid southward propagation over the South China Sea to gravity-wave motions based on the speed and isallobaric angle of wind vectors. Leathers (1986) suggested that the rapid speed could be identified with an orographic Kelvin wave. The second event was a slower-moving positive pressure increase and temperature drop that followed the initial pressure pulse. Chang *et al.* suggested advection as the mechanism for the southward propagation of the second event in the pressure surge. The propagation speed estimated in Fig. 9 is consistent with the 13 m $s^{-1}$ estimation in Fig. 2, and with an 11 m $s^{-1}$ estimate of Chang *et al.* (1983) based on irregularly spaced station data from 25°N to 5°N from the winter of 1978/79. All of these are consistent with a 15 m $s^{-1}$ estimation of Leathers using the same time period as Chang *et al.* with points further north (35°N to 29°N). As both the east Asian background and surge-

associated lower-tropospheric winds are northerly, a nonlinear advective mechanism might seem plausible for the southward propagating pressure surges and associated temperature and wind anomalies.

To examine the advection hypothesis, the meridional-wind anomaly is shown in Fig. 9(b) along the same meridian as considered in Fig. 9(a). The SLP anomaly is reproduced to simplify comparison. The maxima in meridional wind speed are not in quadrature with the temperature or pressure extrema, as would be necessary if nonlinear advection were the primary mechanism. In addition, the maximum meridional wind speed varies along the surge path and is inconsistent with the observed steady southward propagation. The temperature and pressure perturbations associated with negative pressure anomalies are accompanied by southerly-wind anomalies. Under the advection mechanism, negative pressure anomalies and positive temperature anomalies should show northward movement, instead there appears to be southward phase propagation. Southward phase propagation of negative pressure anomalies is observed in both the pressure anomalies of Fig. 2 and the regression of Fig. 9. Further, the negative pressure anomalies also move southward at the same speed as the surges. The observed propagation speed is faster than both the background meridional velocity and the anomalous meridional velocity, also inconsistent with nonlinear advection as a mechanism for the movement of pressure surges.

In contrast to the advection hypothesis, Hsu (1987) and Tilley (1990) have suggested the southward propagation of surges to be due to a topographic Rossby wave, also termed a 'shelf wave' (Pedlosky 1987), the atmospheric equivalent to the oceanic 'continental-shelf wave' (Mysak 1980). Leathers (1986) suggested that advection explained the southward movement of the negative temperature anomalies but hypothesized that the shelf-wave mechanism explained the dynamics of the pressure perturbations. Through this mechanism, the slope of the orography from the east Asian coast to the Himalayas provides an augmented gradient of potential vorticity which acts as a restoring force for perturbations induced either up or down the slope. As in the general atmospheric Rossby-wave case, shelf waves are unidirectional; in the northern hemisphere they propagate with the greater orographic heights to their right.

The evidence presented here supports the hypothesis that pressure-surge propagation over continental east Asia may be related to the dynamics of shelf waves. The consistent southward propagation, with the increasing orographic height to the right, observed in Figs. 2 and 9, and the coincident relationship between SLP and meridional-wind anomalies support the hypothesis, based on theoretical discussions by Pedlosky and by Mysak. As discussed by Pedlosky, the theoretical spatial scale of the shelf wave in the direction normal to the orography is the scale of the slope. The horizontal scale of the pressure anomaly seen in Fig. 5 appears to be consistent with the hypothesis that the slope from the Himalayas to the east Asian coast is the appropriate spatial scale for the pressure and wind anomalies over east Asia during a pressure surge. In addition the vertical structure, considered below, lends further support to the shelf-wave hypothesis.

### *(d) Vertical structure*

Latitude–height cross-sections of meridional-wind and air temperature along 110°E regressed against the SLP base point of 15°N, 115°E are shown in Fig. 10. The northerly meridional-wind anomalies (Fig. 10(a)) associated with the surge occur between 22.5°N and the equator and extend up to 700 hPa. The positive meridional-wind anomalies also proceeding southward have similar dimensions, though only those anomalies between 30°N and 35°N exceed a statistically-significant correlation of 0.2. Significant low-level southerly anomalies develop on subsequent days (Fig. 5). Above 500 hPa, significant subtropical southerlies occur between 27.5°N and 5°N at 200 and 300 hPa. In subsequent

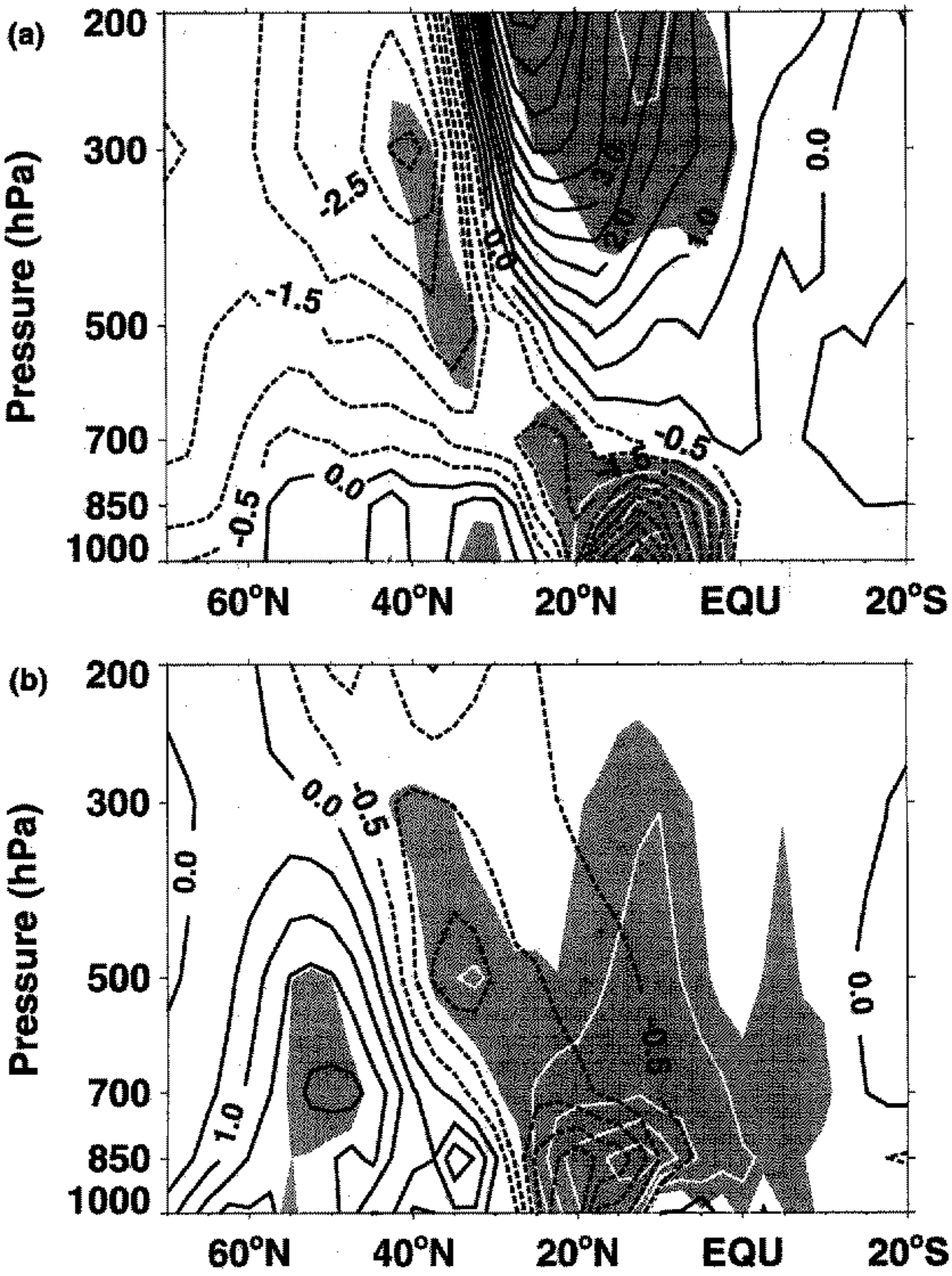


Figure 10. 6- to 30-day bandpass filtered (a) meridional wind (0.5 m $s^{-1}$ contour interval) and (b) air temperature (0.5°C contour interval) as functions of latitude and height along 110°E linearly regressed about sea-level pressure (SLP) at 15°N, 115°E for day 0 corresponding to Fig. 5. The contours represent the regressed value for a typical perturbation of SLP (3.0 hPa) at the base point. The white contours with shading represent the magnitude of the correlation coefficient with a contour interval of 0.1 and a minimum contour value of 0.2.

days, the lower-tropospheric northerlies decrease in intensity (Fig. 5), while the upper-level southerlies appear to increase in response to the convective anomalies, as shown in Fig. 7.

While the regressed meridional-circulation anomalies have distinct lower-tropospheric and upper-tropospheric signals over the whole of east Asia, the temperature anomalies (Fig. 10(b)) appear coherent from the surface to above 500 hPa in the midlatitudes, but are shallower towards the equator. The positive temperature anomaly associated with negative pressure anomalies (compare with Fig. 9(a)) extends to 500 hPa. North of 30°N,

the mid-tropospheric negative temperature anomaly lags behind the anomaly near the surface, reflecting the separation between the near-surface surge and the upper-level wave activity. South of 30°N, the negative temperature anomaly at 850 hPa is collocated with the meridional-wind anomalies, and has approximately the same vertical extent, but at 1000 hPa negative anomalies less than −0.5°C terminate at 10°N. Cross-sections taken over the centre of the South China Sea (115°E, not shown) indicate that the 0.5°C temperature perturbation has maximum southward extent to only 15°N at 1000 hPa and 10°N at 850 hPa. The low-level warming of the surge over the open water is probably due to air–sea interaction modifying the near-surface cold-air anomaly. Thus, as originally observed in two cases by Chang *et al.* (1979), the near-surface temperature signal associated with a pressure surge has deep tropical penetration only near and over the land region of the Indo-China Peninsula. Over the South China Sea, the cold air is quickly modified, and the near-surface signal is lost.

Comparing Fig. 10(a) and 10(b), the vertical change in the phase relationship between the temperature and meridional-wind anomalies south of 45°N is consistent with the hypothesis that different dynamical mechanisms may govern the southward propagation of the anomalies. The vertical structure of the meridional-wind anomalies seen in Fig. 10(a) appears similar to the predicted effect of stable stratification on barotropic shelf-wave structure, as modelled numerically by Wang and Mooers (1976) and Huthnance (1978). Both studies demonstrated that intermediate stratification combined with a sloped bottom surface induces bottom trapping of the velocity anomalies. In Fig. 10(a), the vertical extent of the meridional-wind anomalies in the lower troposphere is confined to near the surface. While not considered in either modelling study, the limited vertical extent of the lower-tropospheric temperature anomaly (Fig. 10(b)) does appear consistent with the hypothesis of bottom trapping.

## 5. Discussion and conclusions

The results found above corroborate some earlier findings on pressure surges, however significant differences have also been found. We now attempt to develop a more consistent morphology of surges by answering the questions posed at the beginning of the paper.

(i) *What are the time-scales associated with surge activity?*

East Asian pressure surges are the dominant mode of submonthly variability in the east Asian winter monsoon system. The spectral results of Figs. 3 and 4 demonstrate a regional localization of statistically-significant power in time-scales between synoptic (2 to 6 days), submonthly (6 to 30 days) and the MJO (30 to 70 days). The synoptic time-scale has little significant variance south of 25°N, suggesting that penetrating pressure surges occur at a longer time-scale. Spectral analysis demonstrates that peaks in submonthly power significant at the 95% level are localized to an area stretching from the Bay of Bengal to the Philippine Sea and from 30°N to the equator. Comparing the spectra (Fig. 3) with the regression results (Fig. 5), submonthly spectral power has maximum values in the regions found as being along the dominant path for South China Sea surges. The submonthly peaks also extend into the region of the Philippine Sea, with power decreasing east of 140°E. The longitudinal distribution of spectral power suggests that the South China Sea and the Philippine Sea are preferred regions for pressure surges. In both the synoptic and submonthly bands, Murakami (1979) found similar spectral peaks with a single winter record over the South China, Philippine, and East China Seas. The Hovmöller diagrams of Fig. 9 indicate a roughly 15-day periodicity for South China Sea surges, but the spectra

of SLP reveal that, in fact, pressure surges are a relatively broadband phenomena in the submonthly range.

(ii) *What are the basic relationships between surge-associated variables, independent of an arbitrary definition?*

The pressure patterns observed in Figs. 5 and 6 represent the dominant evolution of pressure anomalies during the northern hemisphere cool season. Previous studies using rotated principal-component analysis of SLP found similar patterns to those seen here in the time evolution of pressure perturbations (Hsu and Wallace 1985). Based on the propagation characteristics seen in Figs. 2 and 9, the South China Sea surge signal shows three different regional characteristics as it moves equatorward. North of 45°N, the pressure and temperature signals are in quadrature, as would be expected from eastward moving baroclinic waves. Over mainland China, the low-level surge signals in pressure, temperature and wind are almost in phase and appear to propagate much faster than the mean or anomaly advective speed would explain. The vertical structure of the surge suggests bottom trapping of the low-level surge anomalies (Fig. 10), consistent with the shelf-wave modelling work of Wang and Mooers (1976) and Huthnance (1978). The regression results provide observational support for the hypothesis that surges propagate with a shelf-wave-like mechanism, whereby the augmentation of the potential-vorticity gradient by the sloped surface from the east Asian coast to the Himalayan Plateau acts as the restoring force for a southward propagating disturbance. At the southern Chinese coast, the low-level surge propagation speed becomes much larger and pressure, temperature and wind fluctuations are nearly in phase (Fig. 9). An initial pressure increase rapidly spreads over the whole of the South China Sea (Fig. 9) with meridional-wind anomalies spreading southward at nearly the same rate. In Fig. 9, we estimate the speed of surge propagation after leaving the southern Chinese coast to be 40 m $s^{-1}$. This observation is consistent with the hypothesis that, south of the Chinese coast, the initial response to a pressure surge takes the form of a gravity wave (Lim and Chang 1981; Chang *et al.* 1983; Zhang and Webster 1992). The slower-propagating SLP, temperature and wind anomalies are estimated to propagate southward at 11 m $s^{-1}$.

The 1000 hPa air-temperature perturbation associated with the submonthly pressure surges does not penetrate as far south over the South China Sea as the 850 hPa perturbation (Fig. 10(b)). This statistically-significant modification of the surge temperature anomaly at 1000 hPa corroborates the previous study of Chang *et al.* (1979) that showed, using two case studies, that a decrease in temperature associated with pressure surges was not detectable with station data from islands in the South China Sea. They hypothesized that air–sea interactions quickly modify the temperature of the airmass, leaving only the pressure and wind perturbations.

In Fig. 7, the jet anomalies over the Pacific show an out-of-phase relationship with the jet anomalies directly over east Asia. The structure of the east Asian jet anomalies appears to be closely tied to the subtropical and midlatitude upper-level eastward moving waves that merge off the east Asian coast. These results corroborate the previous studies of the surge relationship to Asian jet anomalies that used shorter records (Chang and Lau 1980, 1982).

The local east Asian Hadley cell is weak before surges commence (Figs. 5(a), 7(a), 8). Strong subsidence, as indicated by the 200 hPa circulation of Fig. 7(c) and positive OLR anomalies in the midlatitudes, occurs following the surge-induced initiation of convection in the south-east Asian region. This result is in contrast to the findings of Chang and Lau (1980), who showed that subsidence in the midlatitudes, associated with the downward branch of the local Hadley cell, increased prior to the surge. Instead, the changes in the

200 hPa circulation divergence field seen in Fig. 8, in conjunction with the presence of a large-scale positive OLR anomaly in the midlatitudes of Fig. 7(c), suggest that the upper-level perturbations to the local Hadley cell follow the surge-induced convective anomalies. In a recent AGCM study, Slingo (1998) also found that the upper-tropospheric branch of the local Hadley cell increased following an increase in convective active over Borneo that was associated with surges.

(iii) *Is the tropical response to pressure surges a robust signal?*

The surge relationship to tropical convection and circulation over the Philippine Sea, South China Sea, Indo-China, and eastern Indian Ocean is a statistically-robust signal using base points over east Asia from 55°N southward. In contrast, the southern-hemisphere signal of enhanced convective activity and westerlies is observed with base points over the East China Sea, Philippine Sea, and the South China Sea south of 20°N. The southern-hemisphere signal is not observed using base points over continental Asia.

A comparison of Figs. 5 and 6 shows that South China Sea surges do not have a significant relationship to the Philippine Sea surges that produce the near-equatorial trade enhancements seen in Fig. 6. The difference between the two figures in the western Pacific suggests that South China Sea surges often occur without a deep tropical Philippine Sea surge event, while strong Philippine Sea surges are more likely to be coincident with a surge that also engulfs the South China Sea.

Figure 5 shows that from the Indo-China Peninsula to the Philippines, and in the Indonesian monsoon regions, convective activity increases following the enhancement of the climatological north-easterly monsoon flow associated with a South China Sea pressure surge. This result compares favourably with the previous results of Houze *et al.* (1981), Johnson and Priegntiz (1981), and Chang and Chen (1992). Our results also corroborate the OLR-based statistical work of Kiladis *et al.* (1994) and Meehl *et al.* (1996), but the area of statistically-significant increased convective activity associated with South China Sea surges seen in Figs. 5 and 6 covers a much larger area than was found in those studies.

The statistically-significant linear association between Philippine Sea surges and western Pacific westerly-wind anomalies appears to lie in the coincident timing and interaction of Philippine Sea surges with westward propagating equatorial disturbances. These westward propagating equatorial disturbances appear similar to the equatorial Rossby waves found by Kiladis and Wheeler (1995). Further study is underway to determine the exact nature of the coincident association between these features and the east Asian pressure surges over the South China Sea and Philippine Sea.

The correlation between surges over the South China Sea and upper-level wave activity showing propagation into the westerly duct region demonstrates that low-level pressure surges are an indicator of large-scale submonthly variability throughout the troposphere (Fig. 7), confirming the similar observational findings of Lau and Lau (1984), Joung and Hitchman (1982), Hsu *et al.* (1990), and Meehl *et al.* (1996).

The robustness and high degree of statistical significance of the results presented here provides strong support for the scenario in which convective activity in the western and eastern Pacific are linked through tropical–extratropical interaction, as observed by Meehl *et al.* (1996) and seen in the AGCM results of Slingo (1998). Combining Figs. 5 and 7, a pressure surge induces an increase in convective activity in the South China Sea. The increase in convective activity coincides with an enhancement of the upper-level Hadley circulation over east Asia and an enhancement of the east Asian jet. Following the eastward extension of the enhanced east Asian jet, upper-level wave activity propagates into the eastern tropical Pacific, with ridges suppressing convective activity, and troughs enhancing convective activity, over several days.

## Acknowledgements

The authors would like to thank Dr C. Torrence, Ms P. Zuidema, Dr K. Weickmann, Dr J. Shukla, and Mr M. Wheeler for helpful comments and discussions on this work. The comments of two anonymous reviewers and the associate editor Dr J. Slingo were extremely valuable in revising and clarifying an earlier version of this manuscript. Computing was performed at the Computing Center of the Program in Atmospheric and Oceanic Sciences at the University of Colorado. This work was supported under the TOGA COARE* project grant through the NOAA Office of Global Programs (DOC NA56GP0230) and the Division of Atmospheric Sciences of the National Science Foundation (ATM-9525860 and ATM-9526030). Data were obtained from the archives of the NOAA Climate Diagnostics Center (http://www.cdc.noaa.gov).

## References

Boyle, J. S. 1986 Comparison of the synoptic conditions in mid-latitudes accompanying cold surges over eastern Asia for the months of December 1974 and 1978. Part I: Monthly mean fields and individual events. *Mon. Weather Rev.*, **114**, 903–918

Boyle, J. S. and Chen, T.-J. 1987 'Synoptic aspects of the wintertime East Asian monsoon'. Pp. 125–160 in *Monsoon meteorology*, Eds. C. P. Chang and T. N. Krishnamurti, Oxford University Press

Chang, C. P. and Chen, J.-M. 1992 A statistical study of winter monsoon cold surges over the South China Sea and the large-scale equatorial divergence. *J. Meteorol. Soc. Japan*, **70**, 287–301

Chang, C. P. and Lau, K.-M. 1982 Short-term planetary-scale interaction over the tropics and midlatitudes during northern winter. Part I: Contrasts between active and inactive periods. *Mon. Weather Rev.*, **110**, 933–946

Chang, C. P. and Lau, K. M. W. 1980 Northeasterly cold surges and near-equatorial disturbances over the Winter MONEX area during December 1974. Part II: Planetary-scale aspects. *Mon. Weather Rev.*, **108**, 298–312

Chang, C. P. and Lim, H. 1988 Kelvin-wave CISK: A possible mechanism for the 30–50 day oscillation. *J. Atmos. Sci.*, **45**, 1709–1720

Chang, C. P. and Lum, K. G. 1985 Tropical–midlatitude interaction over Asia and the western Pacific Ocean during the 1983/84 northern winter. *Mon. Weather Rev.*, **113**, 1345–1358

Chang, C. P., Erickson, J. E. and Lau, K.-M. 1979 Northeasterly cold surges and near-equatorial disturbances over the Winter MONEX area during December 1974. Part I: Synoptic aspects. *Mon. Weather Rev.*, **107**, 812–829

Chang, C. P., Miller, J. E. and Chen, G. T. J. 1983 Gravitational character of cold surges during Winter MONEX. *Mon. Weather Rev.*, **111**, 293–307

Chu, E. W. K. 1978 'A method for forecasting the arrival of cold surges in Hong Kong'. Technical Report 43, Royal Observatory, Hong Kong

Chu, P.-S. 1988 Extratropical forcing and the burst of equatorial westerlies in the western Pacific: A synoptic study. *J. Meteorol. Soc. Japan*, **66**, 549–564

Chu, P.-S. and Frederick, J. 1990 Westerly wind bursts and surface heat fluxes in the equatorial western Pacific in May 1982. *J. Meteorol. Soc. Japan*, **68**, 523–537

Chu, P.-S. and Park, S.-U. 1984 Regional circulation characteristics associated with a cold surge event over east Asia during Winter MONEX. *Mon. Weather Rev.*, **112**, 955–965

Colle, B. A. and Mass, C. F. 1995 The structure and evolution of cold surges east of the Rocky Mountains. *Mon. Weather Rev.*, **123**, 2577–2610

Davidson, N., McBride, J. L. and McAvaney, B. J. 1984 Divergent circulations during the onset of the 1978–79 Australian monsoon. *Mon. Weather Rev.*, **112**, 1684–1696

Ding, Y. 1990 Build-up, air mass transformation and propagation of Siberian high and its relation to cold surge in east Asia. *Meteorol. Atmos. Phys.*, **44**, 281–292

Duchon, C. E. 1979 Lanczos filtering in one and two dimensions. *J. Appl. Meteorol.*, **18**, 1016–1022

* Tropical Ocean and Global Atmosphere programme's Coupled Ocean–Atmosphere Response Experiment

Giese, B. S. and Harrison, D. E. 1990 Aspects of the Kelvin wave response to episodic wind forcing. *J. Geophys. Res.*, **95**, 7289–7312

Houze, R. A., Geotis, S. G., Marks, F. D. and West, A. K. 1981 Winter monsoon convection in the vicinity of North Borneo. Part I: Structure and time variation of the clouds and precipitation. *Mon. Weather Rev.*, **109**, 1595–1614

Hsu, H. H. 1987 Propagation of low-level circulation features in the vicinity of mountain ranges. *Mon. Weather Rev.*, **115**, 1864–1892

Hsu, H. H. and Wallace, J. M. 1985 Vertical structure of wintertime teleconnnection patterns. *J. Atmos. Sci.*, **42**, 1693–1710

Hsu, H. H., Hoskins, B. J. and Jin, F.-F. 1990 The 1985/86 intraseasonal oscillation and the role of the extratropics. *J. Atmos. Sci.*, **47**, 823–839

Huthnance, J. M. 1978 On coastal trapped waves : Analysis and numerical calculations by inverse iteration. *J. Phys. Ocean.*, **8**, 74–92

Johnson, R. H. and Priegnitz, D. L. 1981 Winter monsoon convection in the vicinity of north Borneo. Part II: Effects on large-scale fields. *Mon. Weather Rev.*, **109**, 1615–1628

Joung, C. H. and Hitchman, M. H. 1982 On the role of successive downstream development in East Asian polar air outbreaks. *Mon. Weather Rev.*, **110**, 1224–1237

Keen, R. A. 1982 The role of cross-equatorial tropical cyclone pairs in the southern oscillation. *Mon. Weather Rev.*, **110**, 1405–1416

Kiladis, G. N. and Weickmann, K. M. 1992 Circulation anomalies associated with tropical convection during northern Winter. *Mon. Weather Rev.*, **120**, 1900–1923

Kiladis, G. N. and Wheeler, M. 1995 Horizontal and vertical structure of observed tropospheric equatorial Rossby waves. *J. Geophys. Res.*, **100**, 22981–22997

Kiladis, G. N., Meehl, G. A. and Weickmann, K. M. 1994 Large-scale circulation associated with westerly wind bursts and deep convection over the western equatorial Pacific. *J. Geophys. Res.*, **99**, 18527–18544

Kindle, J. C. and Phoebus, P. A. 1995 The ocean response to operational westerly wind bursts during the 1991–1992 El Niño. *J. Geophys. Res.*, **100**, 4893–4920

Knox, R. A. and Halpern, D. 1982 Long range Kelvin wave propagation of transport variations in Pacific Ocean equatorial currents. *J. Marine Res.*, **40**, 329–339

Kung, E. C. and Chan, P. H. 1981 Energetics characteristics of the Asian winter monsoon in the source region. *Mon. Weather Rev.*, **109**, 854–870

Lau, K. M. 1982 Equatorial responses to northeasterly cold surges as inferred from satellite cloud imagery. *Mon. Weather Rev.*, **110**, 1306–1313

Lau, K. M. and Chang, C. P. 1987 'Planetary scale aspects of the winter monsoon and atmospheric teleconnection'. Pp. 161–202 in *Monsoon meteorology*, Eds. C. P. Chang and T. N. Krishnamurti, Oxford University Press

Lau, N. C. and Lau, K.-M. 1984 The structure and energetics of midlatitude distrubances accompanying cold-air outbreaks over east Asia. *Mon. Weather Rev.*, **112**, 1309–1327

Lau, K. M., Chang, C. P. and Chan, P. H. 1983 Short-term planetary-scale interactions over the tropics and midlatitudes. Part II: Winter-MONEX period. *Mon. Weather Rev.*, **111**, 1372–1388

Leathers, D. L. 1986 'Edge wave characteristics of east Asian cold surges'. Master's thesis, Pennsylvania State University, University Park, PA, USA

Liebmann, B. and Smith, C. A. 1996 Description of a complete (interpolated) outgoing longwave radiation dataset. *Bull. Am. Meteorol. Soc.*, **77**, 1275–1277

Lim, H. and Chang, C. P. 1981 A theory for midlatitude forcing of tropical motions during winter monsoons. *J. Atmos. Sci.*, **38**, 2377–2392

Livezey, R. E. and Chen, W. Y. 1983 Statistical field significance and its determination by Monte Carlo techniques. *Mon. Weather Rev.*, **111**, 46–50

Love, G. 1985 Cross-equatorial influence of winter hemisphere subtropical cold surges. *Mon. Weather Rev.*, **113**, 1487–1498

1985 Cross-equatorial interactions during tropical cyclogensis. *Mon. Weather Rev.*, **113**, 1499–1509

Lukas, R. and Lindstrom, E. 1991 The mixed layer of the western equatorial Pacific Ocean. *J. Geophys. Res.*, **96**, 3343–3357

Madden, R. A. and Julian, P. R. 1994 Observations of the 40–50-day tropical oscillation—a review. *Mon. Weather Rev.*, **122**, 814–837

McBride, J. L. 1987 'The Australian summer monsoon'. Pp. 203–231 in *Monsoon meteorology*, Eds. C. P. Chang and T. N. Krishnamurti, Oxford University Press

McPhaden, M. J., Freitag, H. P., Hayes, S. P. and Taft, B. A. 1988 The response of the equatorial Pacific Ocean to a westerly wind burst in May 1986. *J. Geophys. Res.*, **93**, 10589–10603

McPhaden, M. J., Bahr, F., du Penhoat, Y., Firing, E., Hayes, S. P., Niiler, P. P., Richardson, P. L. and Toole, J. M. 1992 The response of the western equatorial Pacific Ocean to westerly wind bursts during November 1989 to January 1990. *J. Geophys. Res.*, **97**, 14289–14303

Meehl, G. A., Kiladis, G. N., Weickmann, K. M., Wheeler, M., Gutzler, D. S. and Compo, G. P. 1996 Modulation of equatorial subseasonal convective episodes by tropical–extratropical interaction in the Indian and Pacific Ocean regions. *J. Geophys. Res.*, **101**, 15033–15049

Murakami, T. 1979 Winter monsoonal surges over east and southeast Asia. *J. Meteorol. Soc. Japan*, **57**, 133–158

1980 Temporal variations of satellite-observed outgoing longwave radiation over the winter monsoon region. Part I: Long-period (15–30 day) oscillations. *Mon. Weather Rev.*, **108**, 408–426

Murakami, T. and Sumathipala, W. L. 1989 Westerly bursts during the 1982/83 ENSO. *J. Climate*, **2**, 71–85

Mysak, L. A. 1980 Recent advances in shelf wave dynamics. *Rev. Geophys. Space Phys.*, **18**, 211–241

Pedlosky, J. 1987 *Geophysical fluid dynamics*. Springer-Verlag, New York

Ramage, C. 1971 Monsoon meteorology. *Int. Geophys. Ser.*, **15**, Academic Press

Reason, C. J. C. 1994 Orographically trapped disturbances in the lower atmosphere: scale analysis and simple models. *Meteorol. Atmos. Phys.*, **53**, 131–136

Slingo, J. M. 1998 Extratropical forcing of tropical convection in a northern winter simulation with the UGAMP GCM. *Q. J. R. Meteorol. Soc.*, **124**, 27–52

Tilley, J. S. 1990 'On the application of edge wave theory to terrain-bounded cold surges: A numerical study'. PhD thesis, The Pennsylvania State University, University Park, PA, USA

Tomas, R. A. and Webster, P. J. 1994 Horizontal and vertical structure of cross-equatorial wave propagation. *J. Atmos. Sci.*, **51**, 1417–1430

Trenberth, K. E. 1991 Climate diagnostics from global analyses: conservation of mass in ECMWF analyses. *J. Climate*, **4**, 707–722

1992 'Global analyses from ECMWF and atlas of 1000 to 10 mb circulation statistics'. Tech. Report NCAR/TN-373+STR, National Center for Atmospheric Research, Boulder, CO, USA

Trenberth, K. E. and Guillemot, C. J. 1995 Evaluation of the global atmospheric moisture budget as seen from analyses. *J. Climate*, **8**, 2255–2272

Wang, D. P. and Mooers, K. C. N. 1976 Coastal-trapped waves in a continuously stratified ocean. *J. Phys. Ocean.*, **6**, 853–863

Webster, P. J. 1981 Mechanisms determining the atmospheric response to sea surface temperature anomalies. *J. Atmos. Sci.*, **38**, 554–571

1987 'The variable and interactive monsoon'. Pp. 269–330 in *Monsoons*, Eds. J. Fein and P. L. Stephens, John Wiley & Sons, New York

Weickmann, K. M. and Khalsa, S. J. S. 1990 The shift of convection from the Indian Ocean to the western Pacific Ocean during a 30–60 day oscillation. *Mon. Weather Rev.*, **118**, 964–978

Williams, M. 1981 'Interhemispheric interaction during Winter MONEX'. In Proceedings of the International Conference on early results of FGGE and large scale aspects of its monsoon experiment, World Meteorological Organization, Geneva

Wu, M. C. and Chan, J. C. L. 1995 Surface features of winter monsoon surges over south China. *Mon. Weather Rev.*, **123**, 662–680

1997 Upper level features associated with winter monsoon surges over south China. *Mon. Weather Rev.*, **125**, 317–340

Zhang, C. and Webster, P. J. 1992 Laterally forced equatorial perturbations in a linear model. Part I: Stationary transient forcing. *J. Atmos. Sci.*, **49**, 585–607

Zhang, Y., Sperber, K. R. and Boyle, J. S. 1997 Climatology and interannual variation of the east Asian winter monsoon: Results from the 1979–1995 NCEP/NCAR reanalysis. *Mon. Weather Rev.*, **125**, 2605–2619